Low-Temperature Simulation of Hypersonic Melting Ablation and the Observed Wave Patterns

CHING-JEN CHEN* AND SIMON OSTRACH†
Case Western Reserve University, Cleveland, Ohio

Hypersonic melting ablation is approximately simulated at low temperature by use of the similarity parameters, gas Reynolds number and inverse Froude number for dynamic simula- and liquid Peclet number and the viscosity exponent for thermal simulation. In the low-temperature experiments, details of the wave formation are observed. A qualitative description of the melting surface is drawn from experiments performed over a wide range of gas Reynolds and liquid Peclet numbers. Unlike wind-generated water waves the ring waves of tektites are of the "slow wave" type that is defined by Craik.

Nomenclature

A = body force appearing in G, ft/sec^2 $A > 0$ for acceleration and $A < 0$ for deceleration.
c_p = specific heat at constant pressure, Btu/slug°R
E = liquid Eckert number, $U_r^2/c_p(T_r - T_{-\infty})$
G = inverse Froude number or ratio of the body force to pressure force, $G = A\rho L/U_\infty^2\rho_g$
H = gas-liquid interface position
k = thermal conductivity, Btu/ft°R sec
L = characteristic length of the probem, ft
N = index to the liquid viscosity-temperature relation
N_γ = heating parameter, $N = k\beta^n/k_g(Pr_g E_g{}^i)^m$
N_s = Strouhal number, $L/U_\infty t_r$
Pr = Prandtl number, $c_p\bar{\mu}/k$
p = dimensionless pressure, $p/\rho_g U_\infty{}^2$
Re_l = liquid Reynolds number, $\bar{\mu}_g{}^2\rho/\bar{\mu}_r{}^2\rho_g$
Re_g = gas Reynolds number, $U_\infty\rho_g L/\bar{\mu}_g$
r = dimensionless body function R/L
t = dimensionless time
t_r = characteristic time, $L\nu_g/U_\infty\alpha\beta^{2n}$, sec
T = temperature, °R
T_r = characteristic interface temperature, °R, $T_r = (T_\infty + T_{-\infty}N_\gamma)/(1 + N_\gamma)$
U = velocity along x coordinate, fps
U_r = liquid characteristic velocity along x, fps coordinate, $U_r = U_\infty\bar{\mu}_g/\bar{\mu}_r$
u = normalized liquid U velocity U/U_r
u_g = normalized U_g velocity U_g/U_∞
V = velocity along Y coordinate, fps
v = normalized quantity of V, $v = V/U_r\delta$
v_g = normalized gas velocity of V_g, $v_g = V_g/U_\infty\delta$
We = Weber number, $U_\infty{}^2\rho_g L/\Gamma$
x = dimensionless quantity of X, $x = X/L$ distance along the body surface measured from the stagnation point
y = dimensionless quantity of Y normalized by $L\delta$, $y = Y/L\delta$ distance normal to the X coordinate
α = liquid thermal diffusivity, ft^2/sec
β = $Pr\ Re_l$ Liquid Pecet number
Γ = surface tension, slug/sec.^{2}
δ = a scale for the velocity layer, $\delta = (Re_g)^{-0.5}$
θ_g = normalized gas temperature, $\theta_g = (T_g - T_r)/(T_\infty - T_r)$
θ = normalized liquid temperature, $\theta = (T - T_{-\infty})/(T_r - T_{-\infty})$
η = gas-liquid interface
μ = normalized liquid viscosity, $\mu = \bar{\mu}/\bar{\mu}_r$
ρ = liquid density, slug/ft^3

Subscripts and Superscripts

g = gas side
r = reference quantity
$-\infty$ = condition at the interior of the body
∞ = condition at the potential flow

Introduction

IN recent years many experiments of melting ablation in hypersonic flows have been conducted to investigate the possibility of providing heat protection for re-entry vehicles and to study the origin, entry path, and the shape of tektites.[1-3] Many experiments that are conducted in high-temperature environments simulate the stagnation pressure and enthalpy of the actual flight. However, they have the following disadvantages: the operating cost is high, deceleration effects of the entry body either are neglected or cannot be simulated with some exceptions (Chapman and Larson's[1] experiment), details of the motion of the gas-liquid interface cannot be easily observed and recorded, and the duration and the range of the experimental facility are short and limited. Adams, Powers, and Georgie,[2] and Dickey and Haacker[3] conducted ablation experiments in a horizontal facility so that the deceleration force is completely neglected. Chapman and Larson properly considered the effect of body force but no details of the wave motion at the gas-liquid interface were presented.

On the other hand, experiments that simulate hypersonic ablation at low temperatures could possibly eliminate the aforementioned disadvantages and yield useful results for the understanding of aerodynamic ablation. For example: Kubota[4] considered an ice model that simulates the flight conditions at Mach number 5.8. However, he did not present a method that correlates the actual material of the entry body to the ice model at the moderate temperature. Ostrach and McConnell[5] made an analysis to determine the parameters needed for the ablation problem. Although they show that the parameter β is important to the ablation problem, no details of their method of simulation was given. A generalization of the analysis was made by Chen[6] to determine the basic similarity parameters that are needed for a proper simulation of ablation problems at the low temperature.

In this paper the method of simulating hypersonic ablation properly at low temperatures is presented and the wave motion of the gas-liquid interface which was experimentally

Presented as Paper 69-97 at the AIAA 7th Aerospace Sciences Meeting, New York, January 20-22, 1969; submitted February 3, 1969; revision received January 20, 1971. This research was supported by NASA Grant NSG-301. The authors wish to express their appreciation to M. Adams and D. Chapman for the use of their picture in Fig. 7.

* Research Assistant; now Associate Professor, Mechanical Engineering, University of Iowa, Iowa City, Iowa.

† Wilbert J. Austin Distinguished Professor of Engineering, Division of Fluid, Thermal, and Aerospace Sciences.

observed is described in detail. The basic parameters and patterns that characterize the wave motion are discussed.

Similarity Parameters

In order to find the conditions for simulating high-temperature ablation in a low-temperature environment we first have to determine the basic nondimensional parameters that describe the phenomena. These are found from the continuity, boundary-layer, and energy equations for Newtonian fluids with all fluid properties taken to be constant except for the liquid viscosity which is assumed to vary with temperature as $\bar{\mu}/\bar{\mu}_r = (T - T_{-\infty})/(T_r - T_{-\infty})^{-N}$. Dynamic and heat-transfer matching conditions at the interface and the initial and boundary conditions must also be used. Radiation and evaporation effects are neglected and the liquid layer is taken to be thin compared to the characteristic length of the melting body so that Cartesian coordinates can be used. The justification for these assumptions are presented in detail in Ref. 6.

To obtain the dimensionless parameters, the variables are all made dimensionless and normalized so that they are of unit order of magnitude and vary from zero to unit order of magnitude. A number of the characteristic or reference quantities to affect this is not at first obvious and these are then explicitly found in Ref. 6, as presented below and in the Nomenclature, by means of an ordering procedure. Thus, the following substitutions are made in the respective equations for the gas and the liquid,

$$u_g = U_g/U_\infty, \quad v_g = V_g/\delta U_\infty, \quad \theta_g = (T_g - T_r)/(T_\infty - T_r)$$
$$r = R(x)/L, \; u = U/U_r, \; v = V/U_r\delta$$
$$\theta = (T - T_{-\infty}),/(T_r - T_{-\infty}), \quad y = Y/L\delta, \quad x = X/L$$
$$p = P/\rho_g U_\infty^2, \quad \mu = \bar{\mu}/\bar{\mu}_r, \quad \eta = H/L\delta$$

There then results the following dimensionless parameters (see Ref. 6 for details): $N_s = L/U_\infty t_r$ Strouhal number; $Re_g = U_\infty L\rho_g/\bar{\mu}_g$ gas Reynolds number; $Pr_g = c_{pg}\bar{\mu}_g/k_g$ gas Prandtl number; $E_g = U_\infty^2/c_{pg}(T_\infty - T_r)$ gas Eckert number; $G = AL\rho/U_\infty^2\rho_g$ inverse Froude number; $We = U_\infty^2\rho_g L/\Gamma$ Weber number; $Pr = c_p\bar{\mu}_r/k$ liquid Prandtl number; $E = U_r^2/c_p(T_r - T_{-\infty})$ liquid Eckert number; $\beta = PrRe_l$ liquid Peclet number; $Re_l = \rho U_r L\delta_r^2/\bar{\mu}_r$ liquid Reynolds number; $N_\gamma = k\beta^n/k_g(Pr_g E_g{}^j)^m$ heating parameter
where,

$$j = 0, m = 1 \text{ if } Pr_g > 1 > E_g, j = 0, m = \tfrac{1}{2} \text{ if } Pr_g < 1 < E_g$$
$$j = 1, \quad m = \tfrac{1}{2} \text{ if } Pr_g < E_g > 1; \; n = 1 \text{ if } \beta > 1; \; n = \tfrac{1}{2} \text{ if } \beta < 1$$

The physical interpretation of the new and important parameters will now be presented. The parameter G is essentially an inverse Froude number and it denotes the ratio of the deceleration (or acceleration) force to the pressure force. It is positive for accelerations and negative for decelerations.

The parameter β is the liquid Peclet number and is a measure of the relative importance of convection and conduction and also is a measure of the coupling between the equations of motion and the energy equation. Since β is a function only of the gas and liquid properties, it can be determined once and for all for a combination of fluids as a function of temperature. This has been done for several materials of interest and its variation with temperature is presented in figures in Refs. 6 and 7. Representative values are also given in Table 1. From that data it can be seen that for a practical temperature range the liquid Peclet number is of unit order of magnitude or less. Thus, this is a significant parameter.

The heating parameter N_γ is perhaps the most important one obtained from the present analysis. It may be considered to be a generalization of the heating parameter γ first introduced by Ostrach and McConnell.[5] The heating parameter relates the characteristic gas-liquid interface temperature T_r to the given conditions of the problem by $T_r = (T_\infty + N_\gamma T_{-\infty})/(1 + N_\gamma)$ or $N_\gamma = (T_\infty - T_r)/(T_r - T_{-\infty})$. Note that the liquid Reynolds number, liquid Prandtl number, liquid Peclet number, and Strouhal number are all functions of the characteristic interface temperature. The heating parameter determines the characteristic gas-liquid interface temperature which, in turn, helps to determine all the aforementioned parameters and, hence, all the characteristics of the problem. The heating parameter also is a combination of the gas and liquid properties and depends on the temperature through the liquid viscosity.

If the gas (like air) is such that its Prandtl and Eckert numbers are less than unity and the liquid Peclet number is less than or equal to unity, the heating parameter can be simplified to $N_\gamma = (k/k_g)(\beta/Pr_g)^{1/2} = (kc_p\nu/k_g c_{pg}\nu_g)^{1/2}$.

The variation of this parameter with temperature for several materials in combination with air at various pressure levels is presented in Ref. 6. Representative values are also given in Table 1. These data indicate that the heating parameter can vary from an order less than unity to an order greater than unity over the temperature range of interest. This implies that the characteristic gas-liquid interface temperature can be close to the freestream temperature T_∞ as well as to the interior temperature of the melting body $T_{-\infty}$.

Table 1 Sample values of dimensionless parameters

	Sohio oil 650 (ASE65)	Tektite	Kerosene oil	Quartz
Experimental conditions				
h_s Btu/slug		7.9×10^4		2.62×10^5
T_s, T_∞ °R	538	5950	536	10500
$T_{-\infty}$ °R	460	1200	300	1200
P/P_{SL}	1	0.35	1	0.13
M_1	0	10	0	3.4
U_∞, fps	46.2	576	43.3	2300
Reference quantities and parameters				
T_r °R	512	3050	375	5200
N_s	3.24×10^{-6}	5.08×10^{-6}	1.45×10^{-4}	1.35×10^{-3}
N_γ	0.66	1.77	2.145	3.6
N	3	12	3.3	19
Re_l	10^{-3}	3.2×10^{-6}	10^{-5}	2.46×10^{-3}
$\beta = Pr\,Re_l$	7.4×10^{-4}	5.7×10^{-3}	2.5×10^{-2}	7.7×10^{-1}
U_r/U_∞	2.86×10^{-6}	7.56×10^{-7}	1.5×10^{-4}	1.27×10^{-4}
G	-1.25	$0.196 \times g$	-1.15	$0.0496 \times g$
Re_g	2.67×10^4	0.605×10^4	2.214×10^4	1.145×10^3
E_g	1.01×10^{-2}	1.7×10^{-2}	1.95×10^{-3}	4.16×10^{-2}
$E\,Pr$	2.38×10^{-9}	7.95×10^{-8}	4.9×10^{-7}	1.25×10^{-6}
We	2.23×10^2	0.3×10^2	2.7×10^2	

Low-Temperature Simulation

For proper low-temperature simulation of the high-temperature phenomena, both dynamic and thermal similitude must be assured.

A. Dynamic Simulation

Among the dimensionless parameters only Re_g and G are the two for dynamic similarity. In order to simulate the inverse Froude number G the gravitational force A may be utilized by aligning the gravity vector with the direction of the deceleration or acceleration. The magnitude of Re_g and G can be adjusted by the model size L and the approaching velocity U_∞.

B. Thermal Simulation

Perhaps the most difficult conditions to simulate are the thermal conditions. In the literature that reports experiments of ablation at high temperature, it is often stated that the stagnation enthalpy and pressure are needed in the simulation of the actual case of interest. However, we find from the describing equations that besides Re_g and G we need also to simulate Pr_g, N, and β. Since we are essentially in-

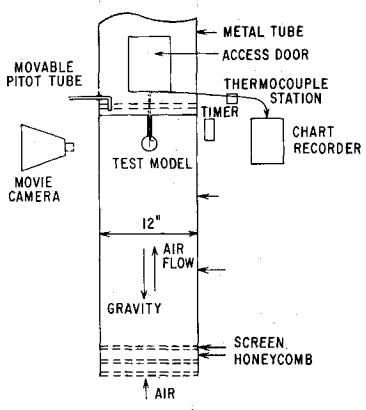

Fig. 1 Experimental set-up.

terested in melting ablation in air, i.e., the Earth's atmosphere, the simulation of gas Prandtl number, Pr_g, is the easiest to achieve because the properties of air keep Pr_g of unit order according to Hansen[8] for a wide range of temperatures from low values to very high ones, even with dissociation and ionization. Hence, the choice of air for the laboratory simulation of the low temperature model is a natural and practical one.

When air is chosen as the gas, we may proceed to search for a liquid material which has a low melting point and yet has the same value of N and β as the material of interest for high-temperature ablation. Recall that heating parameter N_γ determines the characteristic temperature T_r which in turn determines the value of liquid Peclet number β and liquid Reynolds number Re_l. Thus we need to determine a characteristic interface temperature T_r such that the liquid Peclet number β evaluated at T_r for the low-temperature experiment has the same value as the liquid Peclet number in high-temperature ablation. As a consequence there is no need to produce identical stagnation enthalpy or pressure in order to simulate ablation in an experiment.

One has to bear in mind that this simulation requires that the radiation and evaporation effects are negligible. Also for the gas at the high temperature the gas may be dissociated or ionized. Nevertheless, as far as the heat flux and shear effect on the liquid are concerned, Fay and Riddell[9] showed that ionization and dissociation are secondary effects. Hence, admittedly the hypersonic gas boundary-layer phenomena can not be simulated at low temperatures but the melting ablation can be simulated approximately at low temperatures.

When the material chosen does not violate the assumptions made we, therefore, can design an experimental facility to operate near room temperature with a variable freestream velocity so that the gas Reynolds number Re_g and inverse Froude number G can be adjusted to simulate particular problems.

In order to simulate the inverse Froude number G and to satisfy the symmetric condition at the stagnation point a vertical wind tunnel was chosen. The air is driven by a blower through honeycombs and screens from below into a circular, clear plastic test section five feet long with a diameter

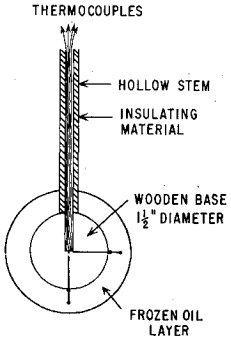

Fig. 2 Low-temperature model.

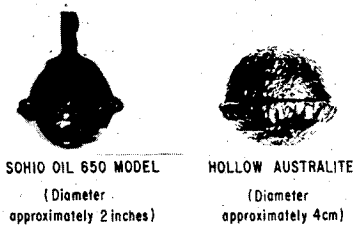

Fig. 3 Tektite and frozen oil model.

of one foot (see Fig. 1). As the direction of the airflow is opposite to the action of the gravitational force the deceleration force is simulated. After the test section of the wind tunnel, the air is guided by a metal tube exhaust into the open air because re-circulation of the heated air to the inlet of the wind tunnel would steadily increase the gas temperature and also would require the use of an oil filter. A small heater was installed in front of the intake of the air to the blower so that the air in the test section could be varied from approximately 70°F to 100°F. A turbulence intensity of one percent was measured by a hot wire anemometer. The air velocity in the test section could be increased up to approximately 100 fps.

To run a test we need, see Fig. 1, a test model, movable pitot tube, thermocouple station, clamp, movie camera, and a time indicator. The pitot tube measures the freestream velocity before the test model is placed into the tunnel. With gas velocity, the properties of the air and test material and the size of the model known, the gas Reynolds number Re_g and inverse Froude number G can be calculated. The thermocouple station, on the one hand, connects all the thermocouples which are imbedded in the model and, on the other hand, connects to the chart recorder so that the response of the test model to the heating and melting can be measured. A 16-mm movie camera was mounted at the side of the test section to take moving pictures of the side view of the test model during the test together with a time indicator on the opposite side of the test section. The recession of the stagnation point with respect to time is then obtained from the film. A thermocouple mounted in the test section to measure the freestream temperature is also connected to the thermocouple station and is also recorded on the chart recorder.

The test model, see Fig. 2, consists of a wooden spherical base mounted on a hollow stem made of insulating material through which the thermocouples which are glued to the spherical base pass and connect to the thermocouple station. The wooden spherical base which is one and one half inches in diameter is then coated with frozen oil layer approximately $\frac{1}{2}$ in. thick so that the model size in the test is approximately varying from two to three inches in diameter. The hollow stem of the model is then fixed by the clamp in the test section during a run.

The coating of the frozen oil layer on the wooden base was accomplished by dipping the base in and out of liquid nitrogen and the testing oil. Each time the model is taken out of the oil can it is spun by hand before it is dipped into the liquid nitrogen so that the oil is uniformly distributed. The method proved to be satisfactory and the model was made as smooth as a mirror-like light bulb because of surface contraction due to surface tension. This was an improvement over McConnell's[10] method of hand molding and spinning in a spherical cavity.

When the model reached the desired size it was placed in a bath containing the nitrogen vapor to bring it to a uniform temperature before the experiment started.

The wind tunnel and the heater were then turned on for approximately ten minutes to allow both freestream velocity and temperature to come to a steady state. The model was then taken out of the temperature bath and clamped into the test section. This took about 5 sec. The time indicator was turned on when the model entered the test section. There was no need to connect the thermocouples of the model to the

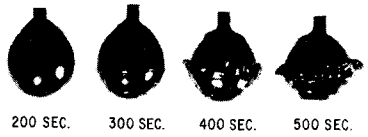

Fig. 4 Evolution of simulated tektite formation.

thermocouple station since they were connected all the time during the making of the model. The moving pictures were taken at intervals with a speed of 16 to 24 frames/sec with Kodak Tri-X film.

Results and Discussion

Figure 3 shows a comparison of the low-temperature frozen oil (Sohio oil 650) model with a tektite which is a typical hollow Australite discovered on Kangaroo Island by Steltzner[11] and photographed by Suess.[12] There is a remarkable similarity between the two. Ring waves similar to those on the tektite are clearly seen on the frozen oil model. This demonstrates that the high-temperature melting phenomena can indeed be simulated by a low temperature experiment. Figure 4 shows four stages of the development of the ring waves on the test model. From the low-temperature experiments we can study further the wave motion in greater detail. Figure 5 shows a plot of the motion of the crest position of the melt wave along the gas-liquid interface vs time for the melting of a Sohio oil model at $Re_g = 2.5 \times 10^4$, $G = -0.88$ and liquid Peclet number β of 4.8×10^{-4}. The dots on Fig. 5 are data taken from the motion pictures which were projected on a film reader frame by frame to trace the subsequent motion of the waves. Several steps of the wave motion are summarized from Fig. 5 as follows. After the model was placed in the tunnel for 60 sec the first visible wave appeared at approximately 20° from the stagnation point with a small amplitude and no appreciable motion downstream. As time increases the wave grows in the amplitude and moves slowly downstream. At 67 sec another wave was observed further downstream at approximately 50° from the stagnation point. This wave was presumably induced by the first wave because the build-up of its amplitude may have distorted the gas flow. The induced waves that are marked by a # in Fig. 5 are rather unstable in comparison with the first wave and soon induce other waves further downstream. As the amplitude of those waves grow, the speed of the wave motion also increases and these waves quickly move downstream to approximately 100° from stagnation point where all waves collide and accumulate. When the accumulation of the melted liquid at this point increases the liquid is broken up and carried away by the air stream. The process is repeated such that the regular waves appear at approximately the 20° position and for every few regular waves an induced wave appears downstream and then both are pushed downstream and accumulated at approximately the 100° position (Fig. 6 shows specifically the history of the motion of the 23rd wave shown on Fig. 5). For this particular case (see Table 1) the average wave length is one half of an inch and the wave speed is 0.01 in./sec.

Examining the entire run of the melting process we see that 1) the frequency of the wave generation increases as time increases because of the increase in the liquid Peclet number β (due to an increase in the interface temperature) which physically means an increase in the melting rate; 2) as a consequence of the increase in the melting rate at large time, as soon as a regular wave appears it moves downstream because it takes less time for the amplitude to build up as compared with the beginning stage; 3) the wave speed also increases with time; 4) the position of generation of the first regular wave seems to advance slightly toward the stagnation point at large time indicating that the change in liquid Peclet number has some effect on the ring wave spacing although the effect is not large.

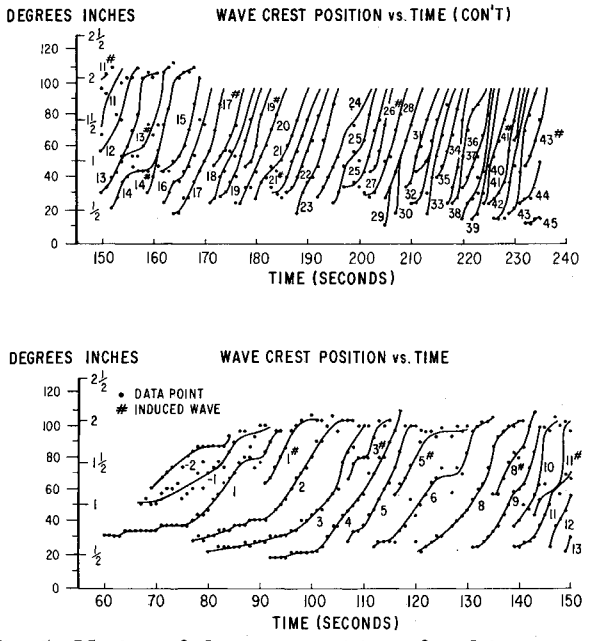

Fig. 5 Motion of the crest position of melting waves.

As the gas Reynolds number increases (to nearly 10^5) the ring waves are readily broken by the airstream as they travel downstream. The last two pictures of Fig. 7 show a comparison of two wave patterns at different values of gas Reynolds number. Furthermore, it is observed that the smaller the inverse Froude number the closer the liquid accumulation will be to the stagnation point.

One of the objectives of the experiments was to try to obtain an understanding of why for the ablation of quartz no waves are discernible whereas ring waves are seen on tektites in contrast. Chapman and Larson[1] in their experimental study on the origin of tektites pointed out that at sufficiently low stagnation pressure, tetktite glass ablates without producing any ring waves but as pressure is increased, ring waves appear first with a rather wide spacing, and then upon a further increase in pressure, with a progressively closer spacing. They also concluded that the variation of the stagnation enthalpy has only a minor effect on the wave spacing. Since it is inconvenient to use dimensional quantities such as pres-

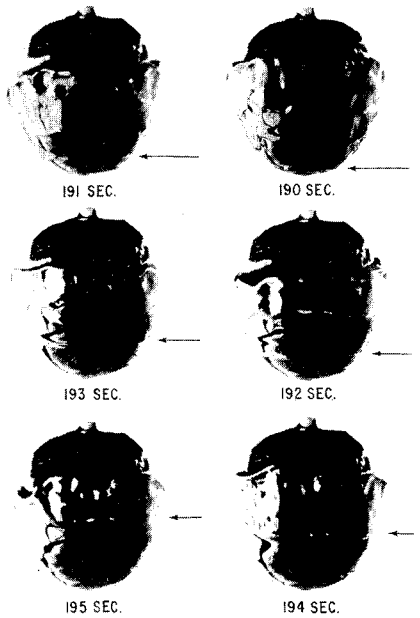

Fig. 6 Motion of the crest position of the 23rd wave.

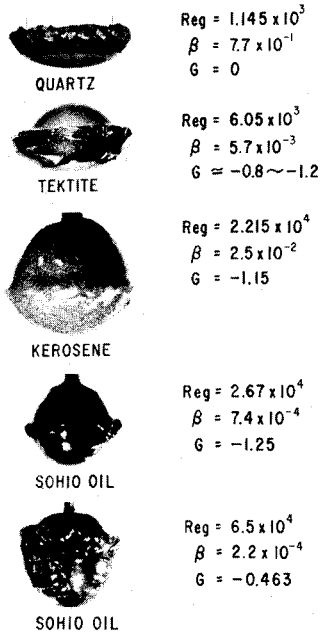

Fig. 7 Comparison of melting surface at different conditions.

sure or enthalpy, the variation of stagnation pressure used by Chapman and Larson[1] can be identified more generally with the present dimensionless parameter, the Reynolds number, while the variation of the stagnation enthalpy is identified with the liquid Peclet number β.

Figure 7 shows a comparison of bodies at different values of gas Reynolds numbers and liquid Peclet numbers from both low and high temperature experiments. The low-temperature experiments are frozen kerosene and frozen Sohio oil 650 whereas the high-temperature experiments are quartz and tektite glass. Examination of these shows that the quartz surface has a smooth interface and the frozen kerosene has a slightly wavy interface marking the inception of the wave formation on the gas-liquid interface. The tektite and frozen Sohio oil models obviously show ring-wave interfaces.

In order to test the conclusions of Chapman and Larson[1] we consider the experiments of quartz and kerosene first. The Reynolds number for the kerosene model is 2.215×10^4 which is higher than that of quartz, 1.145×10^3. The appearance of the small wavy surface for the kerosene model seems to agree with their first conclusion since the larger the Reynolds number the greater the stagnation pressure will be. However, the liquid Peclet numbers for the two are different. The possibility that the waviness of the interface is due to the difference in Peclet number must also be examined. According to their second conclusion the enthalpy has a minor effect on the ring wave spacing. In dimensionless terms this means that the liquid Peclet number has a secondary effect on the instability of the gas-liquid interface. If this were true the difference in Peclet number between quartz and kerosene experiments would not significantly affect the interface and the Reynolds number would be the sole cause of the waviness. However, further comparison with other experiments shows results which contradict their conclusion. Let us compare the kerosene and Sohio oil model, for example. We note that the Reynolds numbers for both experiments are approximately the same whereas the liquid Peclet numbers are different with 2.5×10^{-2} for kerosene and 7.4×10^{-4} for Sohio oil. It is evident now that liquid Peclet number indeed has some effect on the waviness of the gas-liquid interface because the kerosene model shows only a slightly wavy surface whereas the Sohio oil model shows a ring-wave surface with appreciable wave amplitude. Furthermore, when we compare the synthetic tektite glass and kerosene experiments we find that the tektite surface with a smaller Reynolds number, on the contrary, gives a rougher surface than that of kerosene. This is also an indication of the effect of the liquid Peclet number on the waviness of the gas-liquid interface. We, therefore, conclude that both gas Reynolds number and liquid Peclet number indeed significantly affect the gas-liquid interface configuration. This shows that for a wide range of liquid Peclet number Chapman and Larson's[1] second conclusion is not valid.

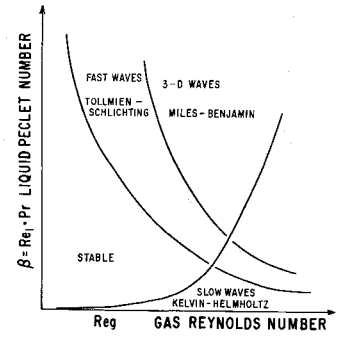

Fig. 8 Wave regimes.

Although the precise mechanism of the inception of melting waves has not been determined, a qualitative picture of the various regimes for waves can perhaps be obtained from Fig. 8 which is a modification of a figure developed by Craik.[13] With gas Reynolds number and liquid Peclet number as coordinates, the figure shows a region of no waves and another region which indicates different types of wave patterns. For small liquid Peclet numbers, as considered herein (see Table 1), there is a critical value of the gas Reynolds number up to which no waves appear. Beyond this critical value slow waves appear. On the other hand, for a fixed gas Reynolds number there is a critical value of the liquid Peclet number above which no waves occur and below which the slow waves are encountered. However, for liquid Peclet numbers greater than unit order the melting liquid flows quite readily. Thus, waves such as encountered in the flow of air over water might be expected. The effect of Froude number would be to shift the demarkation curves but should not change the qualitative picture presented. Thus, it appears that the ring waves obtained on tektites are not of the class obtained by wind flow over water but are of the "slow-wave" type defined by Craik. This contention was made previously by Ostrach and McConnell.[5]

Conclusion

A method of low-temperature simulation of a high-temperature ablation is demonstrated. The basic similarity parameters needed are the gas Reynolds number and inverse Froude number for the dynamic similarity and the liquid Peclet number and viscosity exponent for the thermal similarity. With such low cost experiments run at low temperatures, a wide range of liquid Peclet number can be simulated to investigate the wave motions on the gas-liquid interface.

With the existing experiments a study of the wave patterns shows that both liquid Peclet number and gas Reynolds numbers affect the gas-liquid interface configuration. Furthermore, from the low temperature simulation we conclude that the wave speed increases with increase of the liquid Peclet number and the gas Reynolds number. The effect of the deceleration is to accumulate the melting liquid at a point closer to the stagnation point.

References

[1] Chapman, D. R. and Larson, H. K., "On the Lunar Origin of Tektites," *Journal of Geophysical Research*, Vol. 68, No. 14, 1963, pp. 4305.

[2] Adams, Mac. C., Powers, W., and Georgiev, S., "An Experimental and Theoretical Study of Quartz Ablation at the Stagnation Point," *Journal of the Aerospace Sciences*, Vol. 27, No. 7, July 1960, pp. 535.

[3] Dickey, R. R and Haacker, J. F., "Preliminary Evaluation of a Number of Ablative Heat-Shield Materials Exposed to Combined Radiative and Convective Heating," TM-X-784, 1966, NASA.

[4] Kubota, T., "Ablation with Ice Model at $M = 5.8$," *ARS Journal*, Dec., 1960, pp. 1164.

[5] Ostrach, S. and McConnell, D. C., "Melting Ablation about Decelerating Spherical Bodies," *AIAA Journal*, Vol. 3, No. 10, Oct. 1965, pp. 1883.

[6] Chen, C.-J. and Ostrach, S., "Melting Ablation of Two-Dimensional and Axisymmetric Blunt Bodies with a Body Force," FTAS/TR-67-24, 1967, Case Western Reserve Univ.

[7] Chen, C.-J. and Ostrach, S., "Melting Ablation for Two-Dimensional and Axisymmetric Blunt Bodies with a Body Force, *Progress in Heat and Mass Transfer*, Vol. 2, Pergamon Press, 1969, p. 195.

[8] Hansen, C. F., "Approximation for the Thermodynamic and Transport Properties of High Temperature Air," TN 4150, 1958, NACA.

[9] Fay, J. A. and Riddell, F. R., "Theory of Stagnation Point Heat Transfer in Dissociated Air," *Journal of the Aerospace Science*, Vol. 25, No. 2, Feb. 1958, pp. 73.

[10] McConnell, D. G., "An Investigation of Transient Melting Ablation at the Surface of a Deceleratirn Spherical Body," Ph. D. thesis, 1964, Engineering Div., Case Inst. of Technology.

[11] Steltzner, A. W., "Über Eigenthumliche Obsidian Bomben aus Australia," *Zeitschrift der Deutschen Geologischen Gesellschaft*, Vol. XIV, 1893, pp. 229.

[12] Suess, F. E., "Die Herkinft der Moldavite und Verwandter Glaser," *Jahrbuch d Kaiserlich Königlichen Geologischen Reichsanstalt*, Vol. 50, 1900, pp. 193.

[13] Craik, Alex, D. D., "Wind-Generated Waves in Thin Liquid Films," *The Journal of Fluid Mechanics*, Vol. 26, Pt. 2, 1966, pp. 369–392.

JUNE 1971 AIAA JOURNAL VOL. 9, NO. 6

Head-End Secondary Flows in Solid-Propellant Rockets due to Transverse Acoustic Waves

JEFFERSON Y. S. YANG* AND GARY A. FLANDRO†
University of Utah, Salt Lake City, Utah

The secondary flowfield in the head-end region of solid-propellant rocket motor combustion chamber is derived based on a simplified model. Employing a small perturbation technique, a secondary nonoscillatory perturbation mean flow is generated in a quiescent fluid on an infinite flat plate by the presence of a small amplitude transverse traveling wave motion. Effects of compressibility, variable viscosity, and heat transfer are considered in the study. The first-order oscillatory flow results in a steady mass transport outside of the viscous boundary layer. The secondary perturbation mean flow is found to be a complex three-dimensional spiral motion. The predicted flowfield in this region gives a qualitative explanation of the mechanism of formation of strong axial vortex filament that has been observed in cylindrical combustion chambers during unstable burning.

Nomenclature

a = speed of sound
L = characteristic length
m = wave number and order of Bessel function
P = pressure
r = radial coordinate
t = time
T = temperature
u = velocity
z = longitudinal coordinate
γ = ratio of specific heats
δ = boundary-layer parameter
ϵ = acoustic wave amplitude
η = boundary-layer coordinate
θ = azimuthal coordinate
μ = coefficient of viscosity
ρ = density
σ = Prandtl number
ω = wave frequency

Introduction

SECONDARY flows generated by pressure oscillations in solid rockets may affect motor performance and may produce unexpected forces and moments in flight. Such flows were first treated by Maslen and Moore.[1] The case of severe instabilities that are manifested by a single strong axial vortex filament in chambers with mean flow was first observed in experiments and test firings.[2–5] Later it was studied theoretically by Flandro.[6] He has shown that such effects are caused by the growth of traveling transverse acoustic waves. Hribar[7] studied the interaction of an intense transverse acoustic wave with viscous fluid flow in a cylinder, which is an extension of an earlier work[8] for two-dimensional channel flow.

The influence of the head-end on the characteristics of the rocket motor can be significant as pointed out by Culick[9] but has not been fully accounted for in most analyses. Knowledge of the head-end flowfield is necessary to find the increase in torque on the motor due to angular momentum flux on the head-end; the viscous damping of acoustic oscillations in this region; the mechanism of formation of the strong axial vortex filament and the effects on instrumentation located in the head-end region.

This paper presents an analysis of the rocket motor head-end region flowfield based on a simplified model. An infinite plate in a quiescent fluid is considered. If one precludes the short period of intense combustion instability during which the axial vortex strength reaches a maximum, then the typical mean flow Mach number within the combustion chamber is on the order of 10^{-3}. In the region near the head-end the Mach number is even lower so that the assumption of a quiescent surrounding is reasonable. A transverse traveling wave with a Bessel function form characteristic of wave motion in a cylindrical rocket chamber is then imposed on the fluid. Only the region near the chamber axis is represented in

Received December 29, 1969; revision received August 10, 1970.

* Graduate Research Assistant, Department of Mechanical Engineering.

† Associate Professor, Department of Mechanical Engineering. Member AIAA.